Theoretical study of the multiline EPR signal from the S_2 state of the oxygen evolving complex of photosystem II

Evidence for a magnetic tetramer

Jacques Bonvoisin,* Geneviève Blondin,‡ Jean-Jacques Girerd,‡ and Jean-Luc Zimmermann§

*Centre d'Elaboration de Matériaux et d'Etudes Structurales, Laboratoire d'Optique Electronique, CNRS UPR A 8011, B.P. 4347, 29 rue Jeanne Marvig, 31055 Toulouse; ‡Laboratoire de Chimie Inorganique, Institut de Chimie Moléculaire d'Orsay, CNRS URA 420, Université de Paris Sud, 91405 Orsay; and §Section de Bioénergétique, Département de Biologie Cellulaire et Moléculaire, Centre d'Etudes de Saclay, 91191 Gif-sur-Yvette, France

ABSTRACT The Oxygen evolving complex of plant photosystem II is made of a manganese cluster that gives rise to a low temperature EPR multiline signal in the S_2 oxidation state. The origin of this EPR signal has been addressed with respect to the question of the magnetic couplings between the electron and nuclear spins of the four possible Mn ions that make up this complex. Considering Mn(III) and Mn(IV) as the only possible oxidation states present in the S_2 state, and no large anisotropy of the magnetic tensors, the breadths of the EPR spectra calculated for dimers and trimers with $S = ½$ have been compared with that of the biological site. It is concluded that neither a dinuclear nor a trinuclear complex made of Mn(III) and Mn(IV) can be responsible for the multiline signal; but that, by contrast, a tetranuclear Mn complex can be the origin of this signal. The general shape of the experimental spectrum, its particular hyperfine pattern, the positions of most of the hyperfine lines and their relative intensities can be fit by a tetramer model described by the following six fitting parameters: $g \approx 1.987$, $A_1 \approx 122.4\ 10^{-4}\ cm^{-1}$, $A_2 \approx 87.2\ 10^{-4}\ cm^{-1}$, $A_3 \approx 81.6\ 10^{-4}\ cm^{-1}$, $A_4 \approx 19.1\ 10^{-4}\ cm^{-1}$ and $\delta H = 24.5$ G. A second model described by parameters very close to those given above except for $A_4 \approx 77.5\ 10^{-4}\ cm^{-1}$ gives an equally good fit. However, no other set of parameters gives an EPR spectrum that reproduces the hyperfine pattern of the S_2 multiline signal. This demonstrates that in the S_2 state of the oxygen evolving complex, the four manganese ions are organized in a magnetic tetramer.

INTRODUCTION

The oxidation of water to molecular oxygen by higher plants is catalyzed by a membrane bound protein complex called photosystem II (PS II). A manganese cluster bound to this complex is thought to serve as the prosthetic group where the high electrochemical potential necessary to this reaction is built up; and also where the actual chemistry takes place (1, 2). Four manganese ions are known to be present in PS II, yet the nuclearity of the cluster in the oxygen evolving complex (OEC) and its structure remain largely unknown and are a matter of considerable research efforts in many laboratories.

A number of different techniques have been used to unravel the nature of this Mn cluster. Among these, EPR spectroscopy has proven to yield a wealth of experimental observations on several charge storage states of the enzyme (3–11). In particular, and following the original discovery by Dismukes and Siderer (3), it is well established now that the native S_2 state gives rise to a broad multiline EPR signal centered near $g = 2$ and consisting of at least 19 hyperfine lines (3–7). The similarity of this hyperfine pattern to that observed in the EPR spectra of binuclear mixed valence Mn compounds (12, 13) led to the proposal that a similar binuclear unit may exist for the Mn cluster in the protein (3, 4). In addition, results from XANES and EXAFS spectroscopies (14–20) have demonstrated that, among the four Mn ions associated with the OEC, at least two of them are distant by 2.7 Å, and that the most probable oxidation states of Mn are III and IV. Such a short interatomic distance between two Mn ions is typical for the di-μ-oxo Mn(III)Mn(IV) unit found in the aforementioned mixed valence Mn dimers; thus, the results of x-ray spectroscopy also substantiate a model where the biological Mn cluster is made of a minimal unit in which at least two Mn ions are in close proximity. The EPR properties would result from the magnetic coupling between the two Mn yielding an $S = ½$ spin state that gives rise to the observed multiline signal.

A number of observations however, are indicative of some significant differences between this rather simple model and the biological cluster. First, the X band EPR spectrum from the S_2 state consists of at least 19 lines instead of the 16 lines observed in the spectra of binuclear mixed valence Mn(III)Mn(IV) dimers, and the overall breadth of the signal is larger ($>1,800$ vs $\approx 1,250$ G). The origin of this difference could be

Address correspondence to Jean-Luc Zimmermann.

Abbreviations used in this paper: PS II: Photosystem II, OEC: Oxygen evolving complex, XANES: X-ray absorption near-edge structure, EXAFS: Extended x-ray absorption fine structure, CW EPR: Continuous wave electron paramagnetic resonance, tacn′: *N,N′,N″*-trimethyl-1,4,7-triazacyclononane, tren: 2,2′,2″-triaminotriethylamine, bipy: 2,2′-bipyridine, EGTA: ethylenebis(oxyethylenenitrilo)tetraacetic acid, Sig II_{slow}: the EPR signal from the stable tyrosyl radical Tyr D· of photosystem II, HWHM: Half width at half maximum.

0006-3495/92/05/1076/11 $2.00

g-anisotropy, as is observed for instance in a number of mixed valence Mn(II)Mn(III) dimers (21, 22), but measurements at Q band seem to have ruled out this possibility (5). Second, close observation of the multiline signal shows that the hyperfine lines are broader and that substructure can be resolved on top of these major lines (23, 24). The line width of an EPR line from a metal site in a protein is often larger than that of a corresponding model compound. This is in particular due to unresolved hyperfine couplings from protons in the surrounding protein matrix and also due to strains from the biological environment. However, the dinuclear Mn sites in *Thermus thermophilus* (25) and *Lactobacillus plantarum* (26) pseudocatalase give rise to a 16 lines EPR signal whose linewidth is much shorter than that of the OEC (1). In addition, superhyperfine interactions from chlorine (24) and nitrogen (27, 28) ligands have been ruled out as the origin of the partially resolved substructure seen in the major hyperfine lines, but these features could arise from slight anisotropy of the g or A tensors, resulting to the nonexact superposition of the hyperfine lines in a powder pattern; but they could equally well originate from small hyperfine couplings from more remote ^{55}Mn nuclei, as for example in a higher nuclearity complex. Third, and as mentioned above, in most EXAFS reports, the Mn shell at 2.7 Å fits to a number of scatterers that corresponds to more than one such Mn · · · Mn interaction (16–19), a result which may indicate the presence of a metal site with higher nuclearity in the OEC. In addition, the existence of a third backscattering shell at 3.3 Å which may include Mn has now been confirmed (17–19). This has been interpreted as indicating that trimers or tetramers of Mn could also model the EXAFS data from the OEC (17–19).

More recently, different lines of evidence have led Boussac et al. (29, 30) to suggest that the metal site in the S_2 and S_3 states that are perturbed by a treatment with EGTA is at least a manganese trimer. In addition, recent EPR data obtained in PS II membranes inhibited with ammonia have led Kim et al. (31) to propose that under these conditions the multiline signal originates from a tetranuclear Mn cluster.

Various suggestions have been put forward in the literature that favor trimeric or tetrameric structures for the Mn cluster in the unperturbed OEC. Results from x-ray absorption spectroscopy are the basis of most of these proposals (16–19), however, no unique picture regarding the structure of the Mn complex can be drawn from these data and their interpretation is still debated. On the basis of EPR simulations, Dismukes et al. (32) have proposed that a tetramer made of 3 Mn(III) and one Mn(IV) could model the EPR spectrum of the S_2 state. However, the calculated spectrum failed to reproduce the breadth of the experimental spectrum and the number of the hyperfine lines. In fact, few reports have attempted to rationalize possible structures of the OEC with the EPR data (4, 9, 32–34), mainly because the simulation of the EPR spectrum becomes very complex and seriously under parametrized when dealing with more than two interacting Mn ions. In this paper, we use a simple spin coupling scheme to demonstrate that the multiline EPR signal from the S_2 state cannot be explained by either a Mn dimer or a Mn trimer. A simulation using four different hyperfine coupling constants that reproduces most of the features of the multiline signal is presented and the significance of this result to other data in the literature is discussed.

EXPERIMENTAL

O_2-evolving PS II membranes were prepared from spinach using published procedures (35) and an EPR sample was made using material resuspended at high chlorophyll concentration (≈15 mg/mL). Advancement to the S_2 state was achieved by continuous illumination using an 800-W tungsten lamp while the sample was maintained at 200 K in an ethanol/solid CO_2 slurry (7). The EPR spectrum was recorded on a Bruker ER 300 spectrometer (Bruker Spectrospin SA, Wissembourg, France) operating at X band and fitted with an Oxford continuous flow liquid helium cryostat (Oxford Instruments, Paris, France). EPR data were recorded and then transferred to a laboratory PC and reformatted to allow comparison with the calculated spectra.

Simulation of EPR spectra was done using a FORTRAN program originally developed by Drs L. K. White and R. L. Belford at University of Illinois. The program simulates powder spectra for $S = ½$ systems and can include four different hyperfine interactions using perturbation theory. It was modified to allow for calculation of the hyperfine contributions to the spectra to the 2nd order (see e.g., 36). Briefly, for each transition the resonant field was calculated using perturbation theory to the 2nd order for the hyperfine coupling terms, and the resulting stick spectrum was then convolved with Gaussian lineshape functions. All the calculations done in this work were done using isotropic parameters (see below).

The fit to the EPR spectra was obtained on a VFX ALLIANT minicomputer. The simulation program described above was used together with the MINUIT routine which minimizes the $R = \Sigma_{i=1,n}(y_i^{cal} - y_i^{exp})^2/\Sigma_{i=1,n}(y_i^{exp})^2$ using SIMPLEX and MIGRAD. For this purpose, the experimental spectrum was digitized to give $n = 812$ experimental points with y_i^{exp} as ordinates. The y_i^{cal} are the ordinates of the calculated points for the same field values. The variables of the minimization were the isotropic g value, the four isotropic hyperfine coupling constants A_1, A_2, A_3, and A_4, and the linewidth δH of the EPR line.

RESULTS

Fig. 1 shows the multiline EPR signal from the S_2 state of the OEC recorded at X band. This signal has an original sigmoidal shape and 18 major lines separated by 70–90 G are clearly visible that extend from ≈2,500 to ≈4,200

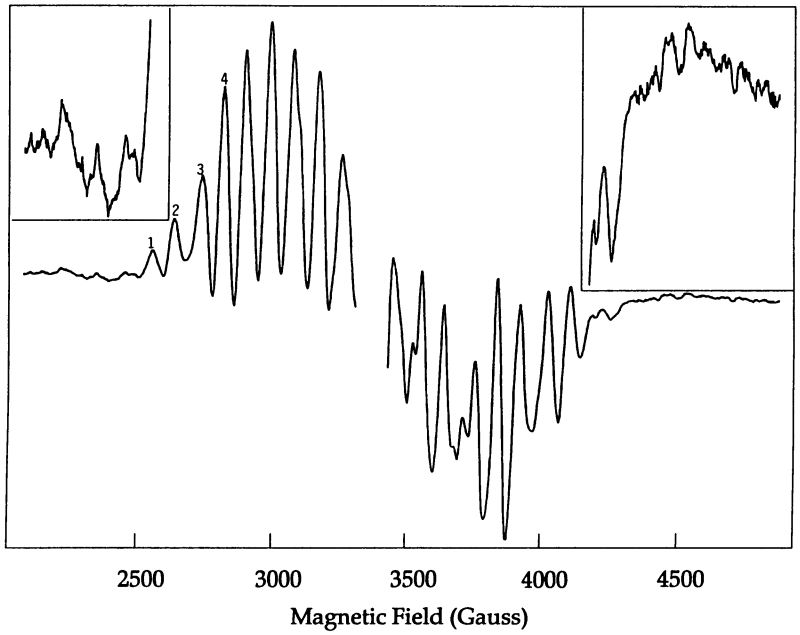

FIGURE 1 The multiline EPR signal from the S_2 state of the OEC recorded under the following conditions: microwave frequency: 9.44 GHz, temperature: 8 K, modulation amplitude: 20 G, modulation frequency: 100 kHz, microwave power: 20 mW. The inserts show the wings of the spectrum expanded by a factor of 8.

G. An extra line is presumably present in the region of the spectrum near $g = 2$ that is excised in Fig. 1 due to the superimposition of Sig. II_{slow}, the sharp signal from $Tyr_D^{\cdot}$, the stable tyrosyl radical of PS II with unknown function. In addition, there is some indication of extra lines being present in the wings of the spectrum below 2,500 G and beyond 4,200 G (Fig. 1 *insert*). Thus, the spectrum spreads over at least 1,800 G.

Hansson et al. (5) have measured the S_2 multiline signal at three different X band frequencies and at Q band (34 GHz). The hyperfine pattern of this signal was found unchanged and the g values of at least 10 peaks were found virtually identical, indicating little, if any, anisotropy of the g tensor (5). More recently however, Diril et al. (22) studied two Mn(II)Mn(III) dimers and found that the g and A tensors are very anisotropic but only the g_z component is resolved in the EPR spectra at X and Q band. They suggested that a similar property may be exhibited by the S_2 EPR multiline signal. If this is actually the case, then the pattern of lines in the multiline signal results from hyperfine interactions being resolved along only one principal axis, with the hyperfine structure for the g_x and g_y components being broadened to the point of not contributing significantly to the observed EPR spectrum (22). A number of points are relevant to this question: first, the Mn(II)Mn(III) dimers that were studied are characterized by rather small exchange coupling constants ($\approx 10\ cm^{-1}$) and it is highly probable that the large anisotropy in the g and A tensors originates from the mixing of sublevels with $S_{eff} = \frac{1}{2}$ from the low lying excited states into the pure $S = \frac{1}{2}$ ground state. This contradicts the behavior of all known complexes made of Mn(III) and Mn(IV) which exhibit rather isotropic g and A tensors (e.g., 13, 37). As noted below other lines of evidence indicate that only Mn(III) and Mn(IV) are present in the OEC in the S_2 state. Second, the unusually large hyperfine coupling constants ($\approx 250 \cdot 10^{-4}\ cm^{-1}$) due to Mn(II) that are derived from the EPR spectra may also be a consequence of the nonpure nature of the EPR active doublet. And third, the resolution of only one component of the g and A tensors in the EPR spectrum would hardly be reconcilable with the observation of hyperfine anisotropy in the wings of the spectrum (38, see below). Thus, the argument of Diril et al. (22) may not apply here.

On the other hand, Rutherford (38) observed the multiline signal produced in two-dimensionally ordered multilayers of PS II membranes. Significant orientation dependence was found in the wings of the spectrum, especially shifts could be observed for the peaks labeled 1 through 4 in Fig. 1, however no obvious change could be detected in terms of peak shifts for the other lines. In particular, the positions of the other ten central main lines were not changed by the orientation (A. W. Rutherford, personal communication). This indicates that the shape and hyperfine pattern of the S_2 multiline

signal shown in Fig. 1 does not result from the superimposition of the different multiline patterns that would exist in a significantly anisotropic EPR signal.

The multiline EPR signal has also been measured at *S* band (3.9 GHz). The breadth of the spectrum was found identical to that measured at *X* band, but 40 to 50 lines could be resolved with spacings of 20–25 G (39). This increased complexity of the signal was partly attributed to increased resolution due to a decrease in *g* strain broadening at *S* band, whereas hyperfine anisotropy was also suggested to be the origin of the orientation dependence of the hyperfine lines (39). On the other hand, the *X* band EPR spectra of a number of di-μ-oxo Mn(III)Mn(IV) dimers have been nearly perfectly simulated and the simulation parameters used for the best fit invariably show significant anisotropy in the *A* tensor, especially in that A_i set that corresponds to the Mn(III) ion (a computation of the EPR spectrum of $[Mn(III)Mn(IV)O_2(tren)_3]^{3+}$ yielded $|A_\parallel| \approx 128 \cdot 10^{-4}$ cm^{-1} and $|A\perp| \approx 150 \cdot 10^{-4}$ cm^{-1} for the Mn(III) hyperfine coupling constants (13), corresponding to local coupling constants of $|a_\parallel| \approx 64 \cdot 10^{-4}$ cm^{-1} and $|a\perp| \approx 75 \cdot 10^{-4}$ cm^{-1} (see below). Although the presence of *A* anisotropy does not change either the number of major lines or the breadth of the signal at *X* band, it leads to splitting of lines and resolution of additional lines through the EPR spectrum at *S* band, as evidenced by the calculation of the EPR spectra (J. L. Zimmermann, unpublished observations). From the evidence outlined above, we consider that more dramatic anisotropy of the *A* tensor that would bias the conclusions drawn from calculations performed using isotropic parameters is rather unlikely. Thus, the *g* and *A* tensors used in calculating the EPR spectra were taken as isotropic.

The magnetic properties of a system consisting of *n* interacting ions can be described by the following hamiltonian (40):

$$H = \sum_i (\beta H \cdot g_i \cdot S_i + I_i \cdot a_i \cdot S_i + S_i \cdot D_i \cdot S_i) - \sum_{i>j} J_{ij} S_i \cdot S_j \quad (1)$$

where β is the Bohr magneton, g_i and a_i are the *g* and *a* tensors of ion *i*, D_i is the zero-field splitting tensor of ion *i*, S_i and I_i are its electronic and nuclear spin angular momentum vectors, and J_{ij} represents the isotropic exchange interaction between ions *i* and *j*. Neither antisymmetric nor anisotropic exchange interactions are taken into account in this hamiltonian and this assumption has proven to be valid in the description of the magnetism of most Mn complexes studied so far (41, 42).

The experimental isotropy of the *g* tensor (see above), and the fact that g_{eff} is close to $g_e \approx 2.0023$ both strongly suggest that the spin state of the system that gives rise to the multiline signal is $S = ½$ and also that the zero-field splitting must be small with respect to the exchange interaction (see 4).

If the exchange hamiltonian $\Sigma_{i>j} J_{ij} S_i \cdot S_j$ in Eq. 1 is the dominant term, then its eigenvectors (labeled by the total spin *S*) can be taken as zeroth-order wavefunctions of the total hamiltonian *H* and the other terms considered only as perturbations. Then for each spin state *S* an effective hamiltonian H_S can be written in which the local quantities g_i, D_i, and a_i are transformed into average quantities g_S, D_S, and $A_{i,S}$ (40).

$$H_S = \beta H \cdot g_S \cdot S + S \cdot D_S \cdot S + \sum_i I_i \cdot A_{i,S} \cdot S \quad (2)$$

g_S and D_S can be expressed as linear combinations of the local tensors and the magnetic hyperfine coupling constants $A_{i,S}$ in the coupled system are related to the a_i in the uncoupled representation.

For states with $S = ½$, Eq. 2 simplifies further:

$$H_{1/2} = \beta H \cdot g_{1/2} \cdot S + \sum_i I_i \cdot A_{i,1/2} \cdot S. \quad (3)$$

As stated above, $A_{i,1/2}$ is taken as isotropic and the following relation can be used:

$$\langle + |A_i S_z| + \rangle = \langle + |a_i S_{iz}| + \rangle, \quad (4)$$

where S_z and S_{iz} are the *z* components of the spin of the cluster and of ion *i* respectively. $|+\rangle$ is the wavefunction of the system spin $S = ½, M_S = +½$. Eq. 4 yields:

$$A_{i,1/2} = 2a_i \langle + |S_{iz}| + \rangle \quad (5)$$

To calculate the magnetic hyperfine coupling constants in the coupled system, that will be used in the simulation, we need to calculate first the expectation values of each individual spin $\langle S_{iz} \rangle$. A similar approach has been used to calculated the hyperfine coupling constants and simulate the Mössbauer spectrum of an Fe-S protein (43).

As already mentioned above, different lines of evidence indicate that the average oxidation state of the Mn in the S_2 state of the OEC is III or IV: results from XANES measured near the Mn K-edge (14, 15, 18, 19, 44), water proton relaxivity (R_1) measurements (45), and CW EPR power saturation of Sig II_{slow} measured in different *S* states (46). The investigation performed in the following will therefore be limited to those conformations that contain these formal valences of Mn.

The spin coupling scheme described here will be used to predict theoretical hyperfine patterns that will be compared to those in the experimental spectrum shown in Fig. 1. In addition, considering the difficulty in simulating the experimental multiline signal with two,

three, or four hyperfine parameters, the overall breadth of the S_2 multiline signal ($\Delta H > 1{,}800$ G) will also be used as an additional parameter to be considered by the calculation. We note it the Δ criterion. The breadth of the EPR signal can be related to the $A_{i,1/2}$ set by (for $S = \frac{1}{2}$):

$$\Delta = 5 \cdot \sum_i |A_{i,1/2}| = 10 \cdot \sum_i |a_i \langle S_{iz} \rangle|. \quad (6)$$

This relation is only valid in perturbation to first order for a Mn cluster.

As noted above, only isotropic parameters are considered in this work. It is possible, however, to extend the validity of the Δ criterion in the case of anisotropy in the hyperfine tensor: it is easy to show that the breadth of the EPR spectrum is also governed by Eq. 6, provided that for each x, y, z set of hyperfine coupling constants, only the parameter with the maximum absolute value is considered and used in the equation. Thus, to have an upper limit for the breadth of a calculated spectrum, one needs to find a value for the local coupling constant that represents an upper limit for Mn(III) and Mn(IV). An extensive survey of the literature available on Mn model complexes (see Table 1) shows that some of the largest values for the ^{55}Mn hyperfine coupling constants are found for instance in the following systems $[Mn^{III}Mn^{IV}(\mu\text{-}O)_2(bipy)_4]^{3+}$ (12) ($a_{Mn(III)} = 78 .10^{-4}$ cm^{-1}) and $[Fe^{III}Mn^{III}(\mu\text{-}O)(\mu\text{-}CH_3CO_2)_2(tacn')_2]^{2+}$ (48) ($a_{Mn(III)} = 78. 10^{-4}$ cm^{-1}). Thus, we chose a value of $a' = 80. 10^{-4}$ cm^{-1} (translating to a splitting of a $\approx$ 85 G at $g \approx 2$) for the upper limit of the local coupling constant discussed above.

TABLE 1 Examples of experimental mononuclear hyperfine coupling constants for Mn(III) and Mn(VI) ions*‡

	$a_{Mn(III)}$ (10^{-4} cm^{-1})	$a_{Mn(IV)}$ (10^{-4} cm^{-1})	ref
$[Mn_2O_2(tren)_2]^{3+}$	75 (x, y) 64 (z)	69 (iso)	13
$[Mn_3O_4(bipy)_4Cl_2]^{2+}$		site MnN_4O_2 66 (x, y) 68 (z) site MnN_2O_3Cl 73 (x, y) 67 (z)	37
$[Mn_3O_4(bipy)_4(H_2O)_2]^{4+}$		site MnN_4O_2 66 (iso) site MnN_2O_4 61 (iso)	47
$[FeMnO(CH_3CO_2)_2L_2]^{2+}$	78 (iso)		48
$[Mn_2O_2(CH_3CO_2)L_2]^{2+}$	72 (iso)	72 (iso)	49
$[Mn_2O(CH_3CO_2)_2L_2']^{+}$	75 (iso)	72 (iso)	50
$[Mn_2O_2(bipy)_4]^{3+}$	78 (iso)	74 (iso)	12
$[Mn_2O_2L_2'']^{3+}$	71 (iso)	71 (iso)	51
$[Mn_2O_2L_2'']^{3+}$	73 (iso)	73 (iso)	52

*See also Table VI in reference 22. ‡The sign of the hyperfine coupling constants has not been determined.

Wave functions describing the desired $S = \frac{1}{2}$ state will be written as a function of local spin wave functions. For each wave function, hyperfine values associated with each individual Mn ion will be calculated and the corresponding Δ compared with the experimental breadth of the spectrum.

The metal site in the OEC contains four Mn ions and three basic models are considered that may explain the multiline signal in the S_2 state: (*a*) A Mn dimer with two non interacting Mn monomers. (*b*) A Mn trimer with one non interacting Mn monomer. (*c*) A Mn tetramer: These possibilities will now be considered.

1-Mn dimer: in a Mn(III)Mn(IV) dimer, an $S = \frac{1}{2}$ ground state results when the spins $S_1 = 2$ for Mn(III) and $S_2 = \frac{3}{2}$ for Mn(IV) are antiferromagnetically coupled. This behavior is in fact observed in all such compounds studied so far. The exchange coupling is usually very strong ($|J| \approx 300$ cm^{-1}; 12, 13, 49, 52–55), especially when the coupling is mediated by a double μ-oxo bridge (it is interesting to note that a somewhat weaker exchange coupling constant between Mn(III) and Mn(IV) has been measured in $MnIII(\mu\text{-}O)(\mu\text{-}CH_3CO_2)_2MnIV$ $(tacn')_2(C1O_4)_3$ which contains only one μ-oxo bridge), resulting in a very stabilized $S = \frac{1}{2}$ ground state. The hyperfine coupling constants in the coupled representation, determined by the projections of the individual ions' spins onto the total spin are $A_{Mn(III),1/2} = 2a_{Mn(III)}$ and $A_{Mn(IV),1/2} = -a_{Mn(IV)}$. Because $a_{Mn(III)} \approx a_{Mn(IV)}$ (12, 33, 56), this simple relation results in the partial degeneracy of the expected 36 lines which would result from the coupling of the two ^{55}Mn nuclei with $I = \frac{5}{2}$, and yields a 16 lines EPR spectrum. Also, Eq. 6 gives $\Delta H = 1{,}275$ G, in good agreement with the measured breadth of the spectra of corresponding model compounds (12, 13). By contrast, this value is quite different from $\Delta H = 1{,}800$ G of the EPR spectrum of the S_2 state (32). Judging from this criterion, it is concluded that a Mn(III)Mn(IV) dimer cannot explain this EPR spectrum. This agrees with earlier arguments against Mn dimers as possible origins for the S_2 multiline signal (9, 32, 34).

2-Mn trimer: two Mn configurations can give rise to a $S = \frac{1}{2}$ spin system: a $Mn(IV)_3$ or a $Mn(III)_2Mn(IV)$ trimer.

$Mn(IV)_3$: By contrast to the case of the dimer described above, more than one spin configuration of the three Mn ions can give rise to a final $S = \frac{1}{2}$ system. In the present case where $S_1 = S_2 = S_3 = \frac{3}{2}$, two configurations with $S = \frac{1}{2}$ occur in the coupled system. These may be obtained by coupling S_1 and S_2 to an intermediate spin $S' = 1$ or 2 and then coupling S' with S_3. Using the kets

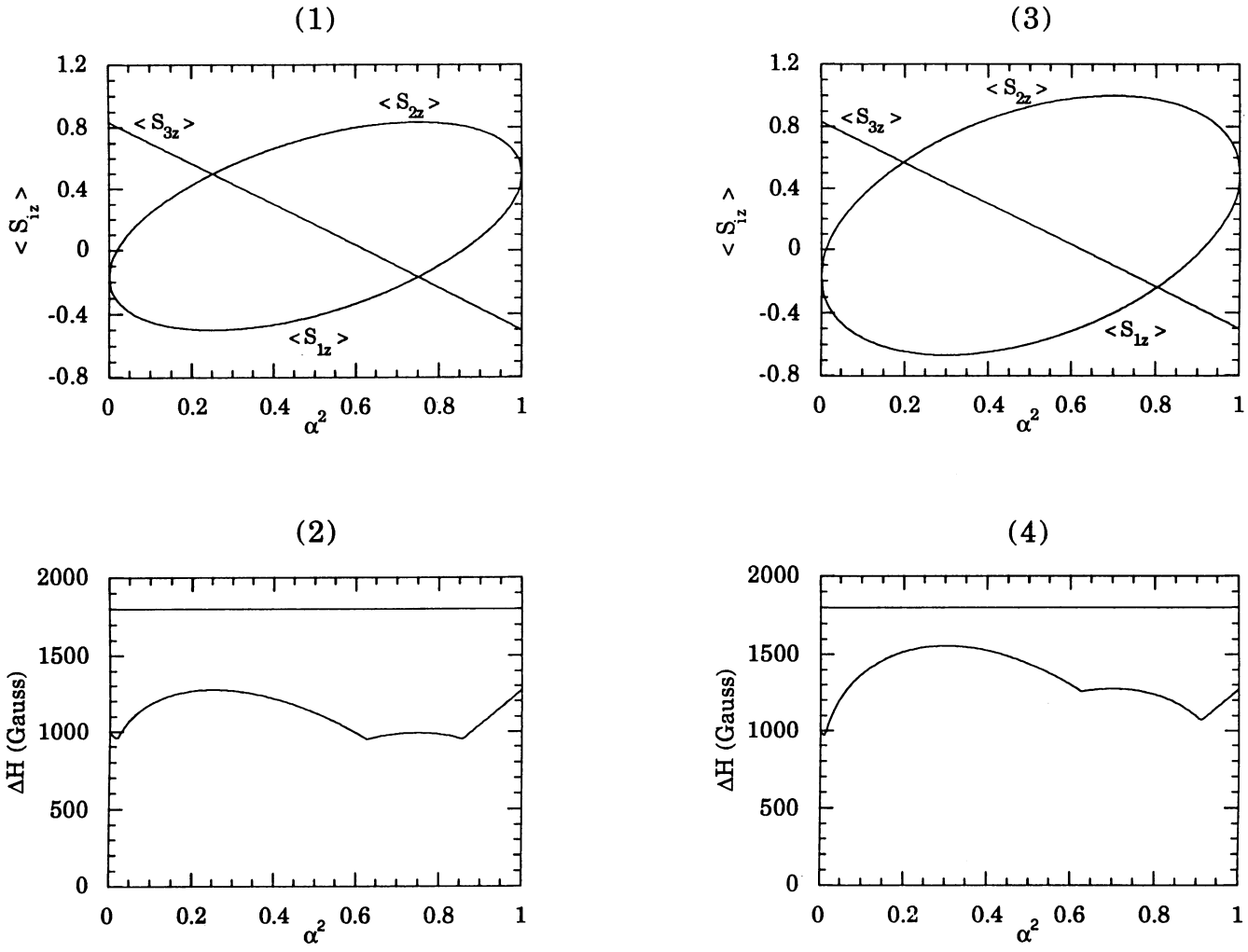

FIGURE 2 Mean values of the z components of the local spins (1) and corresponding spectral breadth (2) as functions of the mixing parameter α^2 in the doublet states for a $Mn(IV)_3$ cluster. The spectral breadth was calculated using a_i = 85 G (see text); (3) and (4) are the analogous curves for a $Mn(III)_2Mn(IV)$ cluster. The straight lines in (2) and (4) at 1,800 G represent the observed breadth of the multiline signal of the OEC S_2 state.

$|S_1S_2(S')\,S_3;S\,M_S\rangle$ as basis set, we write the most general state with $S = ½$ and $M_S = +½$ as:

$$|+\rangle = (1 - \alpha^2)^{1/2}|S_1S_2(1)S_3;\, ½\, ½\rangle + \alpha|S_1S_2(2)S_3;\, ½\, ½\rangle, \quad (7)$$

in which α is a mixing parameter $-1 \leq \alpha \leq 1$ and the $|+\rangle$ wavefunction has been normalized. The choice of which two spins couple to form S' is arbitrary and does not interfere with the final result.

Using standard techniques (57) to evaluate the matrix elements of S_{iz}, one obtains:

$$\langle S_{1z}\rangle = -⅙ + 2\alpha^2/3 - 2\alpha[3(1 - \alpha^2)]^{1/2}/3$$

$$\langle S_{2z}\rangle = -⅙ + 2\alpha^2/3 + 2\alpha[3(1 - \alpha^2)]^{1/2}/3$$

$$\langle S_{3z}\rangle = ⅚ - 4\alpha^2/3. \quad (8)$$

Fig. 2.1 shows a plot of $\langle S_{iz}\rangle$ versus the square of the mixing parameter. From Eq. 6 and using a = 85 G, we can evaluate the overall breadth of the theoretical EPR spectrum of the calculated $S = ½$ state for a given value of the mixing parameter (Fig. 2.2). Interestingly, a trimer that corresponds to the case studied here has recently been synthesized and characterized (37). This complex displays a perfectly resolved EPR spectrum whose breadth (900 G) corresponds to the limit $\alpha = 0$ studied here. A similar conclusion was drawn from EPR and magnetic susceptibility measurements (37). However it is quite clear that the maximum breadth allowed by this scheme (1,275 G) is well below the breadth of the S_2 multiline signal (Fig. 2.2, *straight line*), demonstrating that a $Mn(IV)_3$ trimer cannot model the EPR signal from the S_2 state.

$Mn(III)_2Mn(IV)$: in this trimer, $S_1 = S_2 = 3/2$ and $S_3 = 2$, and the $S = 1/2$ state in the coupled system can also be a mixture of two configurations. The final wavefunction with $S = 1/2, M_S = +1/2$ may be written in the same way as in Eq. 7. Calculation of the matrix elements gives here:

$$\langle S_{1z}\rangle = -1/6 + 2\alpha^2/3 - \alpha[21(1-\alpha^2)]^{1/2}/3$$

$$\langle S_{2z}\rangle = -1/6 + 2\alpha^2/3 + \alpha[21(1-\alpha^2)]^{1/2}/3$$

$$\langle S_{3z}\rangle = 5/6 - 4\alpha^2/3. \quad (9)$$

Numerical calculation shows that the $|\langle S_{iz}\rangle|$ can be larger here than the corresponding values in the $Mn(IV)_3$ trimer (Fig. 2.3). Yet the Δ criterion cannot still be matched (Fig. 2.4). It is concluded that a magnetic trimer is not a good candidate for modeling the EPR spectrum of the S_2 state of the OEC.

Mn tetramer: the most general case of a magnetic complex made of four Mn ions is rather complicated. The exchange hamiltonian $H_e = \Sigma_{i<j} J_{ij} S_i S_j$ may involve six different exchange coupling constants J_{ij}. The $S = 1/2$ subspace is of dimension 8 for the $Mn(IV)_3Mn(III)$ configuration and 7 for the $Mn(III)_3Mn(IV)$ configuration (the other distributions of Mn(III) and Mn(IV) do not give rise to a final $S = 1/2$ state) (see Table 2). A basis set for this subspace is the set of vectors labeled $|S_{12}, S_{34}, S\rangle$ (see Table 2). H_e has to be diagonalized on this basis set and if, as is generally the case, all the J_{ij} are different, then the $S = 1/2$ ground state wavefunction could be a mixture of 8 (or 7) states. In general also S_{12} and S_{34} are not good quantum numbers since H_e does not commute with either S_{12}^2 or S_{34}^2. Thus, the method outlined above for the trinuclear species where the most general $S = 1/2$ ground state is a mixture of just two states cannot be used here. On the other hand, the problem can be simplified if not all the J_{ij} are different. For instance if we can assume that S_{12}^2 commutes with H_e, then S_{12} is a good quantum number and each $S = 1/2$ state will be a mixture of only two wavefunctions. This will happen for a hamiltonian of the form:

$$H_e = -J_{12}S_1 \cdot S_2 - JS_3 \cdot (S_1 + S_2) - J'S_4 \cdot (S_1 + S_2) - J_{34}S_3 \cdot S_4. \quad (10)$$

In such a limiting case one can use the method of the preceding sections and show that the Δ criterion can be matched (yet it does not mean that it corresponds to a good EPR simulation).

It is rather obvious that such a hypothesis is quite restrictive and most importantly there is at present no experimental evidence to support it. In particular, it is easy to show that simple Mn coupling topologies such as the linear one shown in Scheme 1 have only S as good quantum number.

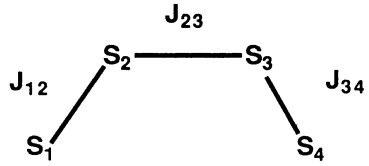

SCHEME 1

We chose to remain as most general as possible and by taking the g and A tensors strictly isotropic, a set of simulation parameters was obtained using the following fitting procedure: For a given set of starting parameters, the EPR spectrum was calculated using the FORTRAN program described in the experimental section, and the residue $R = (y_{th} - y_{exp})^2/y_{exp}^2$ was gradually minimized using SIMPLEX and MIGRAD. Two minima were found with $A_1 = 123.1, A_2 = 87.7, A_3 = 80.9$, and $A_4 = 77.5$ ($.10^{-4}$ cm^{-1}) ($R \approx 0.14$) or $A_1 = 122.4, A_2 = 87.2, A_3 = 81.6$ and $A_4 = 19.1$ ($.10^{-4}$ cm^{-1}) ($R \approx 0.08$). The result of the simulation done using the second set of parameters is shown in Fig. 3. These best two simulations are considered significant because it was found that the minimization was converging towards one of these two minima when starting from any set of fitting parameters (A_1, A_2, A_3, A_4, g and δH). In particular, it was found that no acceptable simulation could be obtained when confining one or more hyperfine coupling constant to zero, thus confirming that a dimer or a trimer of manganese cannot model the S_2 EPR signal.

TABLE 2 **Spin states for a Mn(III)Mn(IV) tetranuclear cluster***

S_{34} \ S_{12}	1/2	3/2	5/2	7/2
0	1/2	3/2	5/2	7/2
1	1/2, 3/2	1/2, 3/2, 5/2	3/2, 5/2, 7/2	5/2, 7/2, 9/2
2	3/2, 5/2	1/2, 3/2, 5/2, 7/2	1/2, 3/2, 5/2 7/2, 9/2	3/2, 5/2, 7/2 9/2, 11/2
3	5/2, 7/2	3/2, 5/2, 7/2, 9/2	1/2,3/2, 5/2 7/2, 9/2, 11/2	1/2, 3/2, 5/2, 7/2, 9/2, 11/2, 13/2
4	7/2, 9/2	5/2, 7/2, 9/2, 11/2	3/2, 5/2, 7/2 9/2, 11/2, 13/2	1/2, 3/2, 5/2, 7/2, 9/2, 11/2, 13/2, 15/2

*For a 3Mn(III) ($S_i = 2$) Mn(IV) ($S_i = 3/2$) cluster, all spin states of this table are possible. For a 1Mn(III) ($S_i = 2$) 3Mn(IV) ($S_i = 3/2$) cluster, the spin states of the last line do not apply.

DISCUSSION

The results of the calculations outlined in the preceding section demonstrate that if only Mn(III) and Mn(IV)

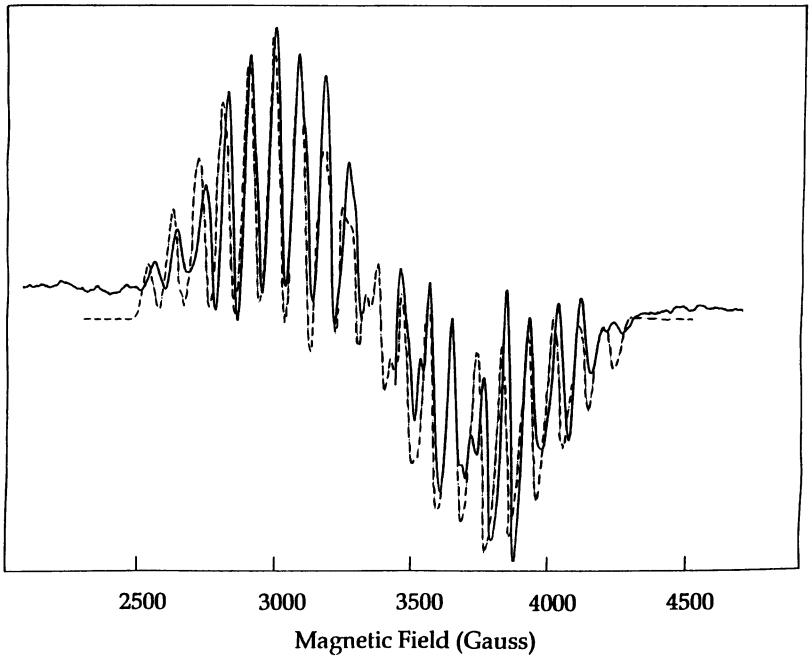

FIGURE 3 The spectrum of Fig. 1 (*solid line*) together with the spectrum calculated using the parameters that gave the best fit: $g_{iso} = 1.987, A1 = 122.4\ 10^{-4}\ cm^{-1}$ (131.9 G); $A_2 = 87.2\ 10^{-4}\ cm^{-1}$ (94.0 G); $A_3 = 81.6\ 10^{-4}\ cm^{-1}$ (88.0 G); $A_4 = 19.1\ 10^{-4}\ cm^{-1}$ (20.6 G), $\delta H = 24.5$ G (HWHM) (*dashed line*).

are to be considered in the OEC in the S_2 state, and no large anisotropy of the g tensor is present, the EPR signal from the S_2 state originates from a magnetic tetranuclear species. This result is of importance for the following reasons: the tetramer model of dePaula et al. (8, 9) was largely based on CW EPR saturation and temperature dependence studies of the multiline signal, however the data have been found to be in error (5 and Britt, R. D. and Zimmermann, J. L., unpublished data). Interestingly, a tetranuclear cluster $Mn(III)_3Mn(IV)$ was also suggested in (32) as a possible origin of the multiline signal of the S_2 state. However our improved experimental data and least square fitting procedure offers a better tetramer simulation than has been previously possible.

There are at present other experimental data that may provide the same conclusion. First, from the analysis of the lineshape and number of lines of the EPR multiline signal from the S_2 state observed when the essential cofactor Ca^{2+} is removed from the OEC by a treatment with EGTA, it has been concluded that the metal site responsible for the signal is at least a trimer of Mn (29); and the EPR signal from the S_3 state which can be detected under these conditions (30) could not be fit with a simple interacting system such as a Mn dimer (unpublished observations, but see legend to Fig. 2 of Ref. 30). This suggests that in the untreated S_2 that gives rise to the multiline signal studied here, the Mn cluster is also bigger than a dimer. And secondly, it has been recently shown that Mn hyperfine structure with regular spacing of $\sim$36 G can be resolved in the $g = 4.1$ signal that arises from the S_2 state under conditions of ammonia inhibition of oxygen evolution (31). This result strongly suggests that both the $g = 4.1$ and multiline signals originate from a Mn tetramer (31), and the conclusions of the present work support this interpretation, at least with respect to the multiline signal.

It is remarkable that the best fit shown in Fig. 3 reproduces most of the spectral features of the S_2 multiline signal. Both signals have a similar S shape which is more pronounced in the high field portion above $g = 2$, the average peak separations are also very similar with most of the hyperfine peaks positions being reproduced. The simulation also predicts the particular hyperfine pattern with the correct relative amplitudes. Closer examination of both signals also reveals that the small differences between the experimental and the simulated signals are nearly exclusively located in the wings of the spectra, i.e. in those regions where hyperfine anisotropy has been suggested to be present (38). It might be expected that a better match with the experimental spectrum could be obtained if anisotropy of the

hyperfine coupling constants and/or a slight anisotropy of the g tensor which would be compatible with the data (5) were considered. As already noted above, significant anisotropy that is presumably present in the A tensor has been suggested to explain the complexity of the S_2 EPR signal measured at S band (39). We are presently working at improving the simulation by introducing anisotropy in the hyperfine tensors.

It has been mentioned that substructure can be resolved in the S_2 multiline signal when working at low modulation amplitudes (23, 24, 28). It is conceivable that this substructure and the increased complexity of the hyperfine pattern in the S band S_2 signal (39) have partly the same origin. The simulated EPR signal shown in Fig. 3 has been obtained by convolution of the individual EPR transitions with Gaussian lineshape functions with linewidths of 24.5 gauss. This leads to an envelope spectrum that masks a large number of narrow lines that can be resolved by using line shape functions with smaller linewidths (not shown). Thus, the set of fitting parameters used to obtain the best fit of the X band EPR signal may also explain the substructure of the signal and the complex hyperfine pattern observed at S band. However, more work is needed to substantiate this possibility.

It is interesting to note that the models associated with the two best fits mentioned above predict four different hyperfine coupling constants, of which one is particular small ($|A| \approx 19.\ 10^{-4}\ cm^{-1}$), when compared to the hyperfine coupling constants of monomeric Mn ions (see Table 1). Such small A values have also been inferred from the analysis of the EPR spectrum of $[Mn(IV)_3O_4(bipy)_4Cl_2]^{2+}$ (37). This demonstrates that a large range of hyperfine coupling constants must be considered when trying to simulate an EPR signal arising from a complex made of more than two interacting Mn Ions.

It is shown in this paper that in the S_2 state of the OEC the four Mn ions are organized in a magnetic tetramer. Two sets of hyperfine coupling constants are obtained that give EPR spectra that are very close to the S_2 EPR signal. These constants do not give, per se, information about the structure of the tetramer, nor about the interactions between the four Mn ions. However, it would be most interesting to derive the coupling schemes (i.e., the exchange coupling constants between the four ions) that are responsible for the particular sets of four hyperfine coupling constants. We are presently working at this problem in our laboratories.

Part of this work was initiated while one of us, J. L. Zimmermann, was a postdoctoral fellow in the laboratory of Prof. K. Sauer and M. P. Klein at University of California at Berkeley, with whom many encouragements and useful discussions are acknowledged. J. L. Z. is supported in part by the CNRS (URA 1290) and during the early part of this work by a grant from NATO (106C86FR). We thank Alain Boussac and Bill Rutherford for critical reading of the manuscript.

Received for publication 12 December 1990 and in final form 19 November 1991.

REFERENCES

1. Sauer, K., V. K. Yachandra, R. D. Britt, and M. P. Klein. 1991. The photosynthetic water oxidation complex studied by EPR and x-ray absorption spectroscopy. *In* Manganese Redox Enzymes. V. L. Pecoraro, editor. VCH Publishers, New York. In press.
2. Rutherford, A. W., J. L. Zimmermann, and A. Boussac. 1992. Oxygen evolution. *In* The Photosystems: Structure, Function and Molecular Biology. J. Barber, editor. In press.
3. Dismukes, G. C., and Y. Siderer. 1981. Intermediates of a polynuclear manganese center involved in photosynthetic oxidation of water. *Proc. Natl. Acad. Sci. USA.* 78:274–278.
4. Hansson, Ö., and L. E. Andréasson. 1982. EPR-detectable Magnetically Interacting Manganese Ions in the Photosynthetic Oxygen Evolving System after Continuous Illumination. *Biochim. Biophys. Acta.* 679:261–268.
5. Hansson, Ö., R. Aasa, and T. Vänngård. 1987. The origin of the multiline and $g = 4.1$ electron paramagnetic resonance signals from the oxygen evolving complex of photosystem II. *Biophys. J.* 51:825–832.
6. Casey, J. L., and K. Sauer. 1984. EPR Detection of a cryogenically photogenerated intermediate in photosynthetic oxygen evolution. *Biochim. Biophys. Acta.* 767:21–28.
7. Zimmermann, J. L., and A. W. Rutherford. 1986. Electron paramagnetic resonance properties of the S_2 state of the oxygen evolving complex of photosystem II. *Biochemistry.* 25:4609–4615.
8. dePaula, J. C., and G. W. Brudvig. 1985. Magnetic properties of manganese in the photosynthetic O_2-evolving complex. *J. Am. Chem. Soc.* 107:2643–2648.
9. dePaula, J. C., W. F. Beck, and G. W. Brudvig. 1986. Magnetic properties of manganese in the photosynthetic O_2-evolving complex. 2. Evidence for a manganese tetramer. *J. Am. Chem. Soc.* 108:4002–4009.
10. Boussac, A., and A. W. Rutherford. 1988. Nature of the inhibition of the oxygen evolving enzyme of photosystem II induced by NaCl washing and reversed by the addition of Ca^{2+} or Sr^{2+}. *Biochemistry.* 27:3476–3483.
11. Boussac, A., J. L. Zimmermann, and A. W. Rutherford. 1989. EPR Signals from modified charge accumulation states of the oxygen evolving enzyme in Ca^{2+}-deficit photosystem II. *Biochemistry.* 28:8984–8989.
12. Cooper, S. R., G. C. Dismukes, M. P. Klein, and M. Calvin. 1978. Mixed valence interactions in Di-μ-oxo bridged manganese complexes. Electron paramagnetic resonance and magnetic susceptibility studies. *J. Am. Chem. Soc.* 100:7248–7252.
13. Hagen, K. S., W. H. Armstrong, and H. Hope. 1988. Isolation of a Bis-Oxo-bridged $Mn^{III}Mn^{IV}$ intermediate by regulated air oxidation. Synthesis, structure and properties of $[Mn_2O_2(tren)_2](CF_3SO_3)_3$. *Inorg. Chem.* 27:969–971.
14. Yachandra, V. K., R. D. Guiles, A. E. McDermott, R. D. Britt, S. L. Dexheimer, K. Sauer, and M. P. Klein. 1986. The state of

manganese in the photosynthetic apparatus. 4. Structure of the manganese complex in photosystem II studied using EXAFS spectroscopy. The S_1 state of the O_2-evolving photosystem II complex from spinach. *Biochim. Biophys. Acta.* 850:324–332.

15. Yachandra, V. K., R. D. Guiles, A. E. McDermott, J. L. Cole, R. D. Britt, S. L. Dexheimer, K. Sauer, and M. P. Klein. 1987. Comparison of the structure of the manganese complex in the S_1 and S_2 states of the photosynthetic O_2-evolving complex: An x-ray absorption spectroscopy study. *Biochemistry.* 26:5974–5981.
16. Guiles, R. D., J. L. Zimmermann, A. E. McDermott, V. K. Yachandra, J. L. Cole, S. L. Dexheimer, R. D. Britt, K. Wieghardt, U. Bossek, K. Sauer, and M. P. Klein. 1990. The S_3 state of photosystem II: Differences between the structure of the manganese complex in the S_2 and S_3 states determined by x-ray absorption spectroscopy. *Biochemistry.* 29:471–485.
17. George, G. N., R. C. Prince, and S. P. Cramer. 1989. The manganese site of the photosynthetic water-splitting enzyme. *Science (Wash., DC).* 243:789–791.
18. Penner-Hahn, J. E., R. M. Fronko, V. L. Pecoraro, C. F. Yocum, S. D. Betts, and N. R. Bowlby. 1990. Structural characterization of the manganese site in the photosynthetic oxygen evolving complex using x-ray absorption spectroscopy. *J. Am. Chem. Soc.* 112:2549–2557.
19. DeRose, V. J., M. J. Latimer, I. Mukerji, V. K. Yachandra, K. Sauer, and M. P. Klein. 1990. Cofactor effects on the photosynthetic oxygen evolving manganese center determined by x-ray absorption spectroscopy. *Proc. 3rd Int. Conference on Biophysics and Synchrotron Radiation.* Stanford, California.
20. Corrie, A. R., M. C. W. Evans, J. A. M. Hubbard, R. W. Strange, and S. S. Hasnain. 1990. An EXAFS study of the manganese oxygen evolving complex of photosystem II. *In* Current Research in Photosynthesis. M. Baltscheffsky, editor. Kluwer Academic Publishers, Dordrecht. I:793–796.
21. Chang, H. R., H. Diril, M. J. Nilges, X. Zhang, J. A. Potenza, H. J. Schugar, D. N. Hendrickson, and S. S. Isied. 1988. An unusually stable $Mn^{II}Mn^{III}$ complex with novel EPR spectra: synthesis, structure, magnetism, and EPR analysis. *J. Am. Chem. Soc.* 110:625–627.
22. Diril, H., H. R. Chang, M. J. Nilges, X. Zhang, J. A. Potenza, H. J. Schugar, S. S. Isied, and D. N. Hendrickson. 1989. Simulation strategies for unusual EPR spectra of binuclear mixed-valence manganese complexes: synthesis, properties, and x-ray structures of the $Mn^{II}Mn^{III}$ complexes $[Mn_2(bpmp)(\mu\text{-}OAc)_2](ClO_4)_2 \cdot H_2O$ and $[Mn_2(bcmp)(\mu\text{-}OAc)_2](ClO_4)_2 \cdot CH_2Cl_2$. *J. Am. Chem. Soc.* 111:5102–5114.
23. Brudvig, G. W., J. L. Casey, and K. Sauer. 1983. Properties of the S_2 state associated with O_2 evolution. *In* The oxygen evolving system of photosynthesis. Y. Inoue, A. R. Crofts, Govindjee, N. Murata, G. Renger, and K. Satoh, editors. Academic Press Inc. Publishers, Tokyo. 159–164.
24. Yachandra, V. K., R. D. Guiles, K. Sauer, and M. P. Klein. 1986. The state of manganese in the photosynthetic apparatus. 5. The chloride effect in photosynthetic oxygen evolution. Is halide coordinated to the EPR-active manganese in the O_2-evolving complex? Studies of the substructure of the low-temperature multiline EPR signal. *Biochim. Biophys. Acta.* 850:333–342.
25. Khangulov, S. V., V. V. Barynin, V. R. Melik-Adamyan, A. I. Grebenko, N. V. Vorvodskaya, I. A. Blumenfeld, S. N. Dobyakov, and V. B. Ilyasova. 1986. EPR study of T-catalase of thermus thermophilus. *Bioorganic Khimica.* 12:741–748.
26. Fronko, R. M., J. E. Penner-Hahn, and C. J. Bender. 1988. EPR spectral evidence for a dinuclear site in the *Lactobacillus Plantarum* manganese catalase. *J. Am. Chem. Soc.* 110:7554–7555.
27. Andréasson, L. E. 1989. Is nitrogen liganded to manganese in the photosynthetic oxygen-evolving system? *Biochim. Biophys. Acta.* 973:465–467.
28. DeRose, V. J., V. K. Yachandra, A. E. McDermott, R. D. Britt, K. Sauer, and M. P. Klein. 1991. Nitrogen ligation to manganese in the photosynthetic oxygen-evolving complex: continuous-wave and pulsed EPR studies of photosystem II particles containing ^{14}N or ^{15}N. *Biochemistry.* 30:1335–1341.
29. Boussac, A., J. L. Zimmermann, and A. W. Rutherford. 1990. Further characterization of the modified S_2 and S_3 EPR signals observed in Ca^{2+}-depleted photosystem-II reconstituted with the 17 and 23 kDa polypeptides. *In* Current research in photosynthesis. M. Baltscheffsky, editor. Kluwer Academic Publishers, Dordrecht. I:713–716.
30. Boussac, A., J. L. Zimmermann, A. W. Rutherford, and J. Lavergne. 1990. Histidine oxidation in the oxygen evolving enzyme. *Nature (Lond.).* 347:303–306.
31. Kim, D. H., R. D. Britt, K. Sauer, and M. P. Klein. 1990. The g = 4.1 EPR signal of the S_2 state of the photosynthetic oxygen evolving complex arises from a multinuclear Mn cluster. *J. Am. Chem. Soc.* 112:9389–9391.
32. Dismukes, G. C., K. Ferris, and P. Watnick. 1982. EPR Spectroscopic evidence for a tetranuclear manganese cluster as the site for photosynthetic oxygen evolution. *Photobiochem. Photobiophys.* 3:243–256.
33. Dismukes, G. C., J. E. Sheats, and J. A. Smegal. 1987. Mn^{2+}/Mn^{3+} and Mn^{3+}/Mn^{4+} mixed valence binuclear manganese complexes of biological interest. *J. Am. Chem. Soc.* 109:7202–7203.
34. Dismukes, G. C. 1986. The organization and function of manganese in the water-oxidizing complex of photosynthesis. *In* Metabolism and Enzyme Function. V. L. Schram, and F. C. Wedler, Eds. Acad. Press, New York, 275–309.
35. Berthold, D. A., G. T. Babcock, and C. F. Yocum. 1981. A highly resolved, oxygen evolving photosystem II preparation from spinach thylakoid membranes. *FEBS (Fed. Eur. Biochem. Soc.) Lett.* 61:231–234.
36. Toy, A. D., S. H. H. Chaston, J. R. Pilbrow, and T. D. Smith. 1971. An electron spin resonance study of the copper(II) chelates of certain monothio-β-diketons and diethyldithiocarbamates. *Inorg. Chem.* 10:2219–2225.
37. Auger, N., J. J. Girerd, M. Corbella, A. Gleizes, and J. L. Zimmermann. 1990. Synthesis, structure and magnetic properties of the stable $[Mn_3^{IV}O_4]^{4+}$ core. *J. Am. Chem. Soc.* 112:448–450.
38. Rutherford, A. W. 1985. Orientation of EPR signals arising from components in photosystem II membranes. *Biochim. Biophys. Acta.* 807:189–201.
39. Haddy, A., R. Aasa, and L. E. Andréasson. 1989. S-band EPR studies of the S_2-state multiline signal from the photosynthetic oxygen-evolving complex. *Biochemistry.* 28:6954–6959.
40. Bencini, A., and D. Gatteschi. 1990. EPR of Exchange Coupled Systems. Springer Verlag, Berlin. 287 pp.
41. Pecoraro, V. L. 1988. Structural proposals for the manganese centers of the oxygen evolving complex: an inorganic chemist's perspective. *Photochem. Photobiol.* 48:249–264.
42. Wieghardt, K. 1989. The active sites in manganese-containing metalloproteins and inorganic model complexes. *Angew. Chem. Int. Ed. Eng.* 28:1153–1172.
43. Kent, T. A., B. H. Huynh, and E. Münch. 1980. Iron-sulfur

proteins: spin-coupling model for three-iron clusters. *Proc. Natl. Acad. Sci. USA.* 77:6574–6576.

44. Kusunoki, M., T. Ono, M. Suzuki, A. Uehara, T. Matsushita, H. Oyanagi, and Y. Inoue. 1990. High-resolution XANES spectra from manganese ions in spinach photosystem II and a proposal for the protein binding sites *In* Current Research in Photosynthesis. M. Baltscheffsky, editor. Kluwer Academic Publishers Dordrecht. I:801–804.
45. Srinivasan, A. N., and R. R. Sharp. 1986. Flash-induced enhancements in the proton NMR relaxation rate of photosystem II particles: response to flash trains of 1–5 flashes. *Biochim. Biophys. Acta.* 851:369–376.
46. Styring, S. A., and A. W. Rutherford. 1988. The microwave power saturation of SII_{slow} varies with the redox state of the oxygen evolving complex in photosystem II. *Biochemistry.* 27:4915–4923.
47. Sarneski, J. E., H. H. Thorp, G. W. Brudvig, R. H. Crabtree, and G. K. Schulte. 1990. Assembly of high-valent oxomanganese clusters in aqueous solution. Redox equilibrium of water-stable $Mn_3O_4^{4+}$ and $Mn_2O_2^{3+}$ Complexes. *J. Am. Chem. Soc.* 112:7255–7260.
48. Bossek, U., T. Weyhermüller, K. Wieghardt, J. Bonvoisin, and J. J. Girerd. 1989. Synthesis, E.S.R. spectrum and magnetic properties of a heterobinuclear complex containing the $[Fe(III)(\mu\text{-}O)(\mu\text{-}CH_3CO_2)_2Mn(III)]^{2+}$ core. *J. Chem. Soc. Chem. Comm.* 633–636.
49. Wieghardt, K., U. Bossek, L. Zsolnai, G. Huttner, G. Blondin, J. J. Girerd, and F. Babonneau. 1987. A novel mixed-valent Mn^{III}-Mn^{IV}-dimer, $[L_2Mn_2(\mu\text{-}O)_2(\mu\text{-}MeCo_2)][BPh_4]_2 \cdot MeCN$: crystal structure, magnetic properties, and E.S.R. spectrum (L = 1,4,7-triazacyclononane). *J. Chem. Soc Chem. Commun.* 651–653.
50. Sheats, J. E., R. S. Czernuszewicz, G. C. Dismukes, A. L. Rheingold, V. Petrouleas, J. Stubbe, W. H. Armstrong, R. H. Beer, and S. J. Lippard. 1987. Binuclear manganese(III) complexes of potential biological significance. *J. Am. Chem. Soc.* 109:1435–1444.
51. Oki, A. R., J. Glerup, and D. J. Hodgson. 1990. Syntheses and characterization of binuclear manganese(III,IV) and -(IV,IV) complexes with ligands related to Tris(2-pyridylmethyl)amine. *Inorg. Chem.* 29:2435–2441.
52. Goodson, P. A., J. Glerup, D. J. Hodgson, K. Michelsen, and E. Pedersen. 1990. Binuclear Bis(μ-oxo)dimanganese(III,IV) and -(IV,IV) Complexes with *N,N'*-Bis(2-pyridylmethyl)-1,2-ethanediamine. *Inorg. Chem.* 29:503–508.
53. Stebler, M., A. Ludi, and H. B. Bürgi. 1986. $[(phen)_2Mn^{IV}(\mu\text{-}O)_2Mn^{III}(phen)_2](PF_6)_3 \cdot CH_3CN$ and $[(phen)_2Mn^{IV}(\mu\text{-}O)_2Mn^{IV}(phen)_2](ClO_4)_4 \cdot CH_3CN$ (phen = 1,10-Phenanthroline): crystal structure analyses at 100 K, interpretation of disorder, and optical, magnetic, and electrochemical results. *Inorg. Chem.* 25:4743–4750.
54. Bashkin, J. S., A. R. Schake, J. B. Vincent, H. R. Chang, Q. Li, J. C. Huffman, G. Christou, and D. N. Hendrickson. 1988. Mixed valence manganese-(II,III) and -(III,IV) dinuclear complexes: preparation, structure, magnetochemistry, and E.S.R. spectra of $Mn_2(biphen)_2(biphenH)(bpy)_2$ and $Mn_2O_2Cl_2(OAc)(bpy)_2$ (biphenH_2 = 2,2'-biphenol, bpy = 2,2'-bipyridine). *J. Chem. Soc Chem. Commun.* 700–702.
55. Wieghardt, K., U. Bossek, J. Bonvoisin, P. Beauvillain, J. J. Girerd, B. Nuber, J. Weiss, and J. Heinze. 1986. Dinuclear manganese(II, III,IV) model complexes for the active center of the metalloprotein photosystem II: synthesis, magnetism and crystal structure of $[LMn^{III}(\mu\text{-}O)(\mu\text{-}CH_3CO_2)_2Mn^{IV}L][ClO_4]_3$ (L = N,N',N''-Trimethyl-1,4,7-triazacyclononane). *Angew. Chem. Int. Ed. Eng.* 25:1030–1031.
56. Bonvoisin, J. 1989. Interaction d'échange dans des complexes polynucléaires de fer et de manganèse d'origine biologique ou synthétique. Etudes Expérimentale et théorique. PhD Thesis. Université Paris-Sud. 216 pp.
57. Brink, D., and G. R. Satchler. 1968. Angular momentum clarendon press. Oxford. 160 pp.